

## TEMPERATURE EFFECT ON THE STRUCTURE OF $\text{NdSr}_2\text{Mn}_2\text{O}_{7+\delta}$ COMPLEX OXIDE

O. M. Fedorova<sup>1\*</sup> and L. B. Vedmid<sup>1,2</sup>

High-temperature X-ray diffraction and differential scanning calorimetry are used to study the features of structural changes in  $\text{NdSr}_2\text{Mn}_2\text{O}_{7+\delta}$  complex oxide at temperatures from room to 1150 °C. Structural calculations by the Rietveld method establish a relationship between anomalies in the temperature dependences of unit cell parameters and in the DSC curves with changes in the lengths of bonds between Mn and Nd, Sr cations and oxygen atoms.

**DOI:** 10.1134/S0022476620120094

**Keywords:** Ruddlesden–Popper phases, X-ray diffraction analysis, differential scanning calorimetry, bond lengths.

## INTRODUCTION

The  $\text{Sr}_3\text{Ti}_2\text{O}_7$  compound was first obtained by S. N. Ruddlesden and P. Popper in 1958 [1]. In this compound, double  $\text{SrTiO}_3$  layers (perovskite type) alternate with the  $\text{SrO}$  layer (rock salt type). The unit cell contains two formula units. The phases with an analogous structure began to be called by their name. Later, the phases with the general formula  $A_{n+1}B_n\text{O}_{3n+1}$  ( $n \geq 1$ ) were synthesized which contained copper, cobalt, iron, manganese instead of titanium and some strontium ions were replaced by rare-earth elements [2, 3]. B.V. Beznosikov and K.S. Aleksandrov clarified the concentration limits of the existence of Ruddlesden–Popper (R–P) phases [4]. The recent interest in phases with the general formula  $\text{Ln}_{2-x}\text{Sr}_x\text{Mn}_2\text{O}_7$ , which belong to the R–P phases with  $n = 2$ , was induced by the discovery of a colossal magnetoresistance effect in them [5]. The physical properties of these compounds have been extensively studied [6–8]. There are studies of the formation of these phases [9, 10], however, structural changes under the effect of external parameters (temperature and oxygen pressure) remain unstudied. Moreover, when the kind of lanthanide-substituting alkaline-earth cations and the lanthanide type change, the structure of these phases can change [11]. In the phases where barium substitutes for some Ln atoms [12], structural transitions were found with increasing temperature. However, there are no works examining the structure of R–P phases with other alkaline-earth elements at high temperatures, although just in the  $\text{NdSr}_2\text{Mn}_2\text{O}_{7+\delta}$  compounds the colossal magnetoresistance effect was revealed [13]. Yet another feature of the R–P phases is also the presence of hyperstoichiometric oxygen atoms that affects the functional properties of these phases [14]. Review [14] discusses the main mechanisms of the oxygen ion migration and the R–P phase stability in the  $A_{n+1}B_n\text{O}_{3n+1}$  system ( $n = 1$ ;  $A = \text{La, Pr}$ ;  $B = \text{Ni, Co, Cu}$ ). It is noted

---

<sup>1</sup>Institute of Metallurgy, Ural Branch, Russian Academy of Sciences, Ekaterinburg, Russia; \*fom55@mail.ru. <sup>2</sup>Ural Federal University, Ekaterinburg, Russia. Original article submitted February 17, 2020; revised July 16, 2020; accepted July 20, 2020.

that the R–P phases with  $n = 2$  exhibit a higher electron conductivity and thermal stability than oxides with  $n = 1$ . Hence, the aim of our work was a more detailed analysis of the structure of  $\text{NdSr}_2\text{Mn}_2\text{O}_{7+\delta}$  in a temperature range from room to +1150 °C in order to determine the temperature ranges of the structural stability of this compound.

## EXPERIMENTAL

The  $\text{NdSr}_2\text{Mn}_2\text{O}_{7+\delta}$  compound was synthesized by the standard ceramic method. The precursors— $\text{Nd}_2\text{O}_3$  (99.8% purity),  $\text{SrCO}_3$  (high purity grade), and  $\text{Mn}_2\text{O}_3$  ( $\geq 98\%$  purity) in equimolar ratios—were mixed in a FRITSCH planetary mill in the ethanol medium; then the mixtures were pressed in pellets with a diameter of 10 mm and a thickness of 1 mm and annealed in a Nabertherm furnace at 1400 °C, with a temperature maintenance accuracy of  $\pm 2^\circ$ . The powder X-ray diffraction (XRD) analysis of the reaction products was performed on a Shimadzu XRD-7000 diffractometer with  $\text{CuK}\alpha$  radiation. The high-temperature XRD studies were carried out on a Shimadzu HA-1001 sample heating attachment with successive heating in a temperature range 20–1150 °C (heating rate 10 deg/min), a 10 min exposition at each temperature, and a subsequent measurement in a 2θ angle range 20–60°, with a step of 0.02 and an exposition of 1.5 s. The full-profile XRD analysis was performed by the Rietveld method using the GSAS software [15]; the model described in [6] was used as the initial one. In this model, the coordinates of Nd1 and Sr1 cations in the perovskite (P) block are 0, 0, 0.5; those in the rock salt (RS) layer are 0, 0, 0.6829; the coordinates of manganese cations are 0, 0, 0.9018; those of the apical oxygen anions O1 are 0, 0, 0 and 0, 0, 0.18 of O2; those of the in-plane oxygen anions are 0, 0.5, 0.0977. For the thermogravimetric investigation a NETZSCH STA 449F Jupiter simultaneous thermoanalyzer was used. The heating was performed in the air with a rate of 10 deg/min from room temperature to 1200 °C. The oxygen nonstoichiometry of  $\text{NdSr}_2\text{Mn}_2\text{O}_{7+\delta}$  was determined by the sample weight loss after its complete reduction to stable oxides in a vacuum circulation device [9].

## RESULTS AND DISCUSSION

According to the powder XRD data, single-phase  $\text{NdSr}_2\text{Mn}_2\text{O}_{7+\delta}$  oxide obtained has the tetragonal structure (space group  $I4/mmm$ ) with unit cell parameters  $a = 3.848(4)$  Å,  $c = 19.976(8)$  Å. Fig. 1 depicts the XRD pattern of this sample at

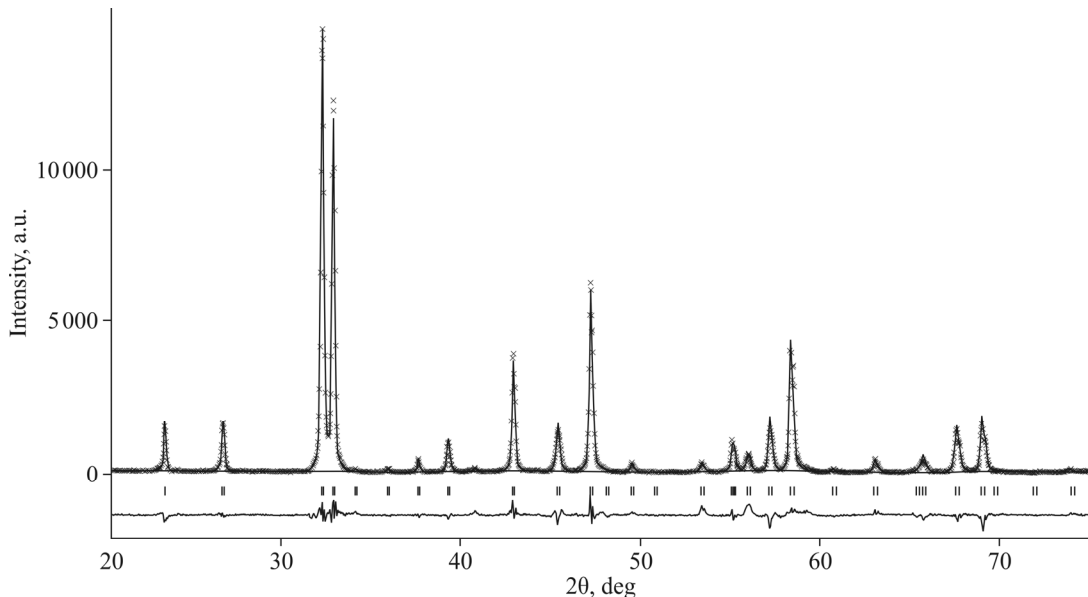


**Fig. 1.** XRD pattern of the  $\text{NdSr}_2\text{Mn}_2\text{O}_{7+\delta}$  sample at room temperature: experiment is designated by crosses, calculation is designated by solid lines, Bragg peak positions are designated by strokes, differential curve is given at the bottom.

room temperature. The oxygen nonstoichiometry of the initial sample is positive (0.22); i.e., the formula of the initial compound can be written as  $\text{NdSr}_2\text{Mn}_2\text{O}_{7.22}$ . Our method of determining the oxygen nonstoichiometry of the samples is characterized by its estimation as the absolute oxygen amount in initial oxide (except for oxygen contained in the dissociation products). Since in perovskite-like manganites oxygen exists in different forms [16], depending on the composition and the method of preparation of the initial sample and it is not possible to distinguish them, we assumed that the weight loss after reduction in hydrogen refers only to removed hyperstoichiometric oxygen ( $\delta$ ), which slightly overestimates the results. We also assumed the absence of significant oxygen nonstoichiometry of the dissociation products ( $\text{MnO}$ ,  $\text{SrO}$ ,  $\text{Nd}_2\text{O}_3$ ) under the conditions of our experiment.

In a temperature range 220–300 °C, the temperature dependences of  $\text{NdSr}_2\text{Mn}_2\text{O}_{7+\delta}$  unit cell parameters and volume demonstrate bends, indicating a structural change in the compound (Fig. 2).

In the DSC curve in the same temperature range, an exothermic effect is observed (Fig. 3), which confirms the powder XRD data. This exothermic effect is accompanied by a small decrease in the sample weight, evidencing a change in the oxygen nonstoichiometry of the  $\text{NdSr}_2\text{Mn}_2\text{O}_{7+\delta}$  phase. In a range 200–400 °C the oxygen nonstoichiometry decreases by 0.36% and the oxygen index becomes 7.19; i.e., the compound formula is  $\text{NdSr}_2\text{Mn}_2\text{O}_{7.19}$ . According to the data from [17], in the R–P phases, oxygen exists in three forms: surface, near-surface, and lattice. The first two forms of oxygen are most active; they are removed before 420 °C. The manganese oxidation state slightly decreases. In [14], it was found that

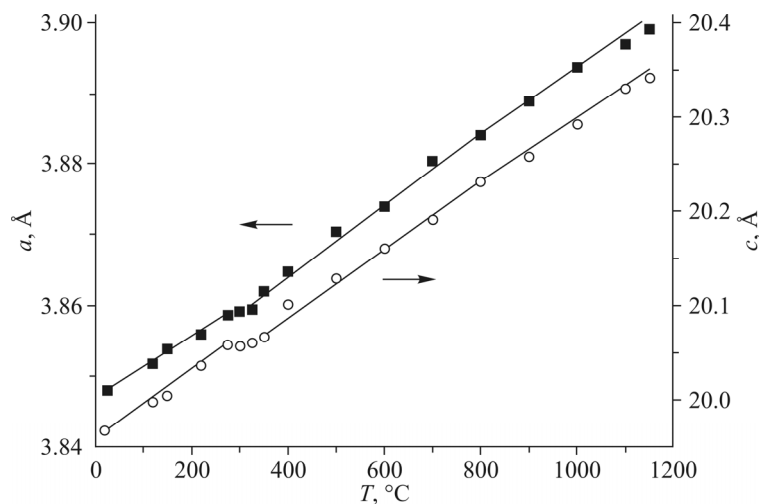


**Fig. 2.** Temperature dependence of the unit cell parameters of  $\text{NdSr}_2\text{Mn}_2\text{O}_{7+\delta}$ .

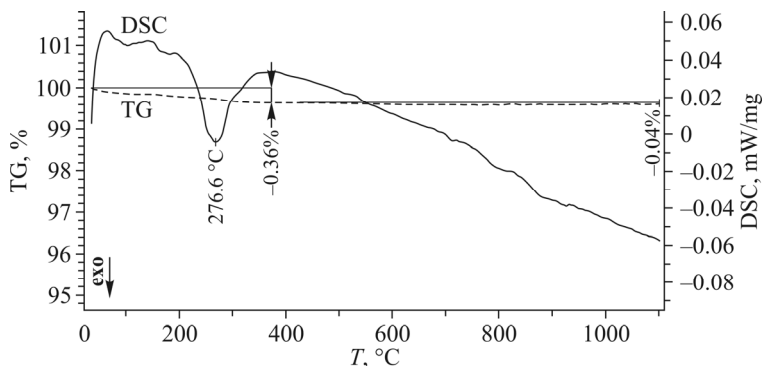


**Fig. 3.** Data of the diffraction scanning calorimetry and thermogravimetry for  $\text{NdSr}_2\text{Mn}_2\text{O}_{7+\delta}$  oxide.

hyperstoichiometric oxygen in the R–P phases was in rock salt layers as interstitial defects; the authors of [18] called this excess oxygen interstitial and also pointed out that it was located in the rock salt layers in the R–P phases. Although these studies were performed on the R–P phases with  $n = 1$ , we suppose that in our phases, hyperstoichiometric oxygen is also located in the blocks with the NaCl structure type.

To explain this behavior of the unit cell parameters and the exothermic effect, the structural calculations of the NdSr<sub>2</sub>Mn<sub>2</sub>O<sub>7+δ</sub> phase by the Rietveld method were performed at temperatures from room to 1150 °C. The results for the bond lengths at temperatures from room to 400 °C are shown in Table 1 (this range was chosen because abrupt changes in the structural parameters occur precisely in this interval, while with a further increase in temperature the parameters linearly increase due to the thermal expansion of the sample). It should be noted that our data at room temperature coincide with the results from [6].

Complex oxide NdSr<sub>2</sub>Mn<sub>2</sub>O<sub>7</sub> is a representative of R–P phases with the general formula (Ln<sub>1-x</sub>A<sub>x</sub>)<sub>n+1</sub>Mn<sub>n</sub>O<sub>3n+1</sub> (Ln is the rare-earth element, A is the bivalent metal cation). These phases are characterized by a coherent intergrowth structure of the blocks with the perovskite structure type (the block consists of n layers) and the blocks with the NaCl structure type [10]. At  $n = 2$  this is the formula of layered manganite NdSr<sub>2</sub>Mn<sub>2</sub>O<sub>7+δ</sub> (a structural fragment of this compound is given in Fig. 4).

In the structure of NdSr<sub>2</sub>Mn<sub>2</sub>O<sub>7+δ</sub> the manganese atoms are surrounded by six oxygen atoms, four of which are located in the Mn–O plane (they are designated as O3), one is above the plane (designated as O1), yet another is below the plane (O2), thus forming a MnO<sub>6</sub> octahedron (Fig. 4).

At room temperature, the Mn–O1 bond length is 2.038 Å and Mn–O2 is 1.798 Å; i.e., the MnO<sub>6</sub> octahedron undergoes a distortion due to the presence of the Mn<sup>3+</sup> ions. In a temperature range 220–270 °C, the Mn–O1 distance first

**TABLE 1.** Calculation Results of the Crystal Structure of NdSr<sub>2</sub>Mn<sub>2</sub>O<sub>7+δ</sub> in a Temperature Range from Room to 400 °C

Parameter	Temperature, °C							
	25	120	150	225	275	300	350	400
<i>a</i> , Å	3.8482(1)	3.8522(2)	3.8558(1)	3.8580(2)	3.8569(3)	3.8603(1)	3.8618(2)	3.8625(1)
<i>c</i> , Å	19.9761(7)	20.0516(8)	20.0519(7)	20.0504(9)	20.0623(7)	20.0634(6)	20.0644(9)	20.1011(7)
(Nd/Sr)1–O1	2.722(2)	2.725(4)	2.726(3)	2.729(2)	2.731(1)	2.742(4)	2.7246(3)	2.733(3)
(Nd/Sr)2–O2	2.575(1)	2.476(1)	2.443(2)	2.442(1)	2.441(2)	2.441(2)	2.331(3)	2.199(2)
(Nd/Sr)2–O2 (экв.)	2.7234(2)	2.7278(1)	2.7283(1)	2.7295(2)	2.7303(2)	2.7374(2)	2.7382(1)	2.7415(1)
(Nd/Sr)1–O3	2.5964(2)	2.6104(1)	2.6369(1)	2.6577(2)	2.6603(2)	2.6764(2)	2.6901(1)	2.7014(1)
(Nd/Sr)2–O3	2.6161(2)	2.6324(2)	2.6511(3)	2.7079(1)	2.7364(2)	2.7561(1)	2.7613(2)	2.7667(2)
Mn–O1	2.039(1)	2.039(1)	2.039(2)	2.0520(1)	2.013(2)	2.038(1)	2.047(2)	2.101(2)
Mn–O2	1.798(2)	1.805(2)	1.864(1)	1.880(1)	1.989(2)	1.946(1)	1.946(2)	2.038(2)
Mn–O3	1.929(1)	1.932(1)	1.933(2)	1.932(2)	1.933(3)	1.932(2)	1.932(2)	1.932(2)
Site occupancy								
Nd1(P)	0.546(2)	0.542(2)	0.481(2)	0.438(2)	0.389(2)	0.377(2)	0.357(2)	0.356(2)
Sr1(P)	0.454(2)	0.458(2)	0.519(2)	0.562(1)	0.611(2)	0.623(2)	0.643(2)	0.644(2)
Nd2(RS)	0.548(2)	0.554(2)	0.565(2)	0.579(2)	0.594(2)	0.618(2)	0.626(2)	0.631(2)
Sr2(RS)	0.452(2)	0.446(2)	0.435(2)	0.421(1)	0.406(2)	0.382(2)	0.374(2)	0.369(2)
Convergence factors								
<i>R</i> <sup>2</sup> , %	8.39	7.42	8.38	9.17	8.11	7.08	8.50	9.37
<i>wR</i> <sub>P</sub> , %	18.3	17.6	16.3	17.1	16.7	17.0	17.3	17.2
<i>R</i> <sub>P</sub> , %	14.0	13.6	12.5	13.2	12.5	12.9	12.1	13.1
$\chi^2$	2.39	2.42	2.38	2.33	2.11	2.16	2.83	2.51

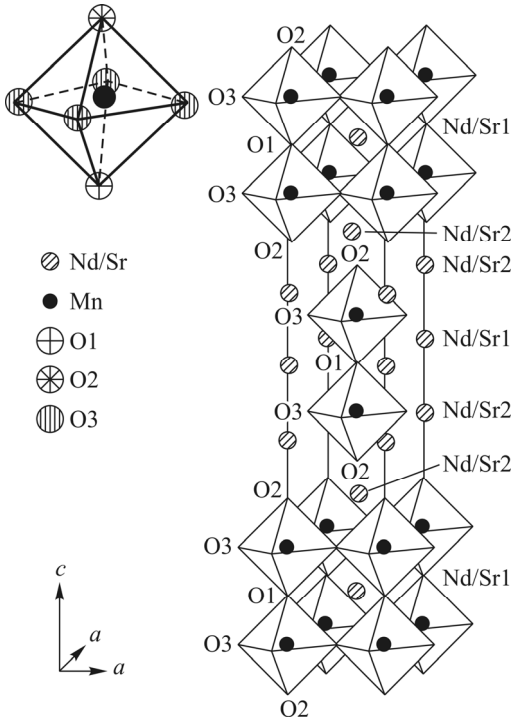


**Fig. 4.** Fragment of the crystal structure of  $\text{NdSr}_2\text{Mn}_2\text{O}_{7+\delta}$  [15].

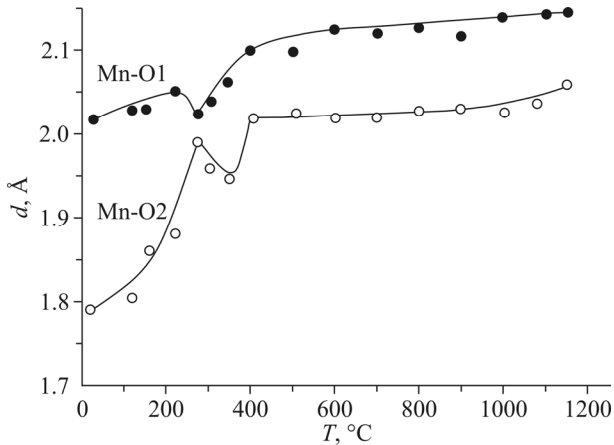


**Fig. 5.** Temperature dependence of Mn–O1 and Mn–O2 bond lengths. The accuracy of determining the bond lengths does not exceed the symbol size.

increases, and at 300 °C decreases; the Mn–O2 bond lengths increase and become almost equal ( $\approx 2.00 \text{ \AA}$ ), which evidences a decrease in the distortion of the  $\text{MnO}_6$  octahedron (Fig. 5). An increase in the temperature from 270 °C to 400 °C is accompanied by oxygen release, which causes an increase in the number of Jahn–Teller  $\text{Mn}^{3+}$  ions leading to an increase in the Mn–O1 bond lengths and a decrease in the Mn–O2 bond lengths; i.e., the  $\text{MnO}_6$  octahedron becomes again less symmetrical due to the Jahn–Teller distortion. Thereafter, the lengths of these bonds smoothly increase up to 1150 °C.

The Nd/Sr atoms are at two positions (Fig. 3). In the perovskite-like blocks, the Nd/Sr1 atoms are surrounded by 12 oxygen atoms (eight O3 atoms and four O1 atoms); in the blocks with the NaCl structure type, Nd/Sr2 atoms are surrounded by nine oxygen atoms (four O3 atoms and five O2 atoms, one of which is apical). With increasing temperature, the Nd/Sr1–O1 bond lengths first increase up to a temperature of 275 °C, then decrease at 300 °C, and increase again up to

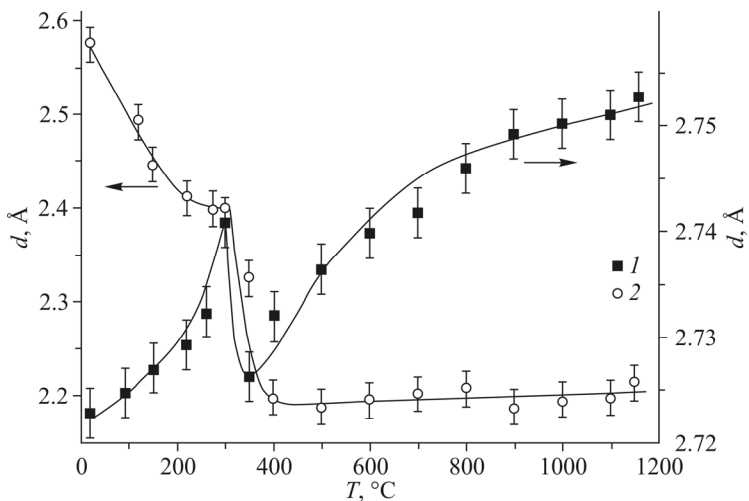


**Fig. 6.** Temperature dependence of Nd/Sr1–O1 (1) and Nd/Sr2–O2 (2) bond lengths.

1200 °C. The distances between Nd/Sr2 and the apical oxygen O2 decrease throughout the entire temperature range studied, but the sharpest jump is observed at 275–400 °C (Fig. 6).

The layered ordering of rare-earth and strontium cations occurs due to increasing oxygen deficiency. This is evidenced by the DSC and TG results. Near 300 °C, these dependences have local minima. The analogous behavior is observed in similar Ba-substituted orthomanganites  $\text{LnBaMn}_2\text{O}_{6-\delta}$  [19].

This behavior of the Nd/Sr1–O1 and Nd/Sr2–O2 bond lengths indicates an increase in the height of the perovskite blocks and a decrease in the blocks with the NaCl structure type. This can be explained as follows: at room temperature the neodymium and strontium ions statistically occupy the same crystallographic positions, without causing a lattice distortion. With increasing temperature, the apical Mn–O bonds elongate in  $\text{MnO}_6$  octahedra; the height of the perovskite blocks increases and the height of the rock salt blocks decreases. To maintain the structure stability, the  $\text{Nd}^{3+}$  and  $\text{Sr}^{2+}$  ions are more orderly distributed over the positions in the crystal structure: the strontium cations with a large ionic radius occupy the positions in the perovskite blocks in a 12-coordinated environment; and the neodymium cations with a shorter ionic radius, in the blocks with the NaCl structure type, with a 9-coordinated environment (Table 1). Our data coincide with the data [20], where it was established that 73% of neodymium ions in the  $\text{Nd}_{1.2}\text{Sr}_{1.8}\text{Mn}_2\text{O}_7$  compound occupied the positions with a 9-coordinated environment of the oxygen ions.

As seen from Table 1, the Nd/Sr1–O3 and Nd/Sr2–O3 bond lengths smoothly increase throughout the entire temperature range due to the thermal expansion of the sample.

## CONCLUSIONS

Thus, in our study it was found that in a temperature range 250–300 °C, in the  $\text{NdSr}_2\text{Mn}_2\text{O}_7$  compound the bond lengths of manganese, neodymium, and strontium cations with oxygen atoms change, which causes a distortion of  $\text{MnO}_6$  octahedra and the structural blocks containing neodymium and strontium ions. However, the space group of complex oxide does not change. It is established that with increasing temperature there is a partial ordering of neodymium and strontium cations over certain positions in the crystal structure of  $\text{NdSr}_2\text{Mn}_2\text{O}_7$  – most neodymium ions occupy the positions in blocks with the NaCl structure type, while most strontium ions occupy the positions in the perovskite blocks.

## FUNDING

The work was performed under the State Task for the Institute of Metallurgy of the Ural Branch of the Russian Academy of Sciences within the Program of Basic Research of State Academies of Science using the scientific instruments of the Collective Equipment Center Ural-M.

## CONFLICT OF INTERESTS

The authors declare that they have no conflict of interests.

## REFERENCES

1. S. N. Ruddlesden and P. Popper. *Acta Crystallogr.*, **1958**, *11*, 54.
2. S. E. Dann and M. T. Weller. *J. Solid State Chem.*, **1995**, *115*, 499.
3. A. P. Galayda, N. E. Volkova, A. A. Startseva, L. Y. Gavrilova, and V. A. Cherepanov. *J. Struct. Chem.*, **2019**, *60*(5), 789.
4. B. V. Beznosikov and K. S. Aleksandrov. *Crystallogr. Rep.*, **2000**, *45*, 792.
5. A. I. Coldea, L. E. Spring, S. J. Blundell, J. Singleton, and W. Hayes. *J. Phys.: Condens. Matter*, **1999**, *11*, 9053.
6. P. D. Battle, M. A. Green, N. S. Laskey, and J. E. Millburn. *Phys. Rev. B*, **1996**, *54*, 15967.
7. R. Seshadri, A. Maignan, M. Hervieu, N. Nguyen, and B. Raveau. *Solid State Commun.*, **1997**, *101*, 4530457.
8. A. M. Yankin, A. V. Fetisov, O. M. Fedorova, S. A. Uporov, and V. Ya. Mitrofanov. *J. Rare Earths*, **2015**, *33*, 282.
9. A. M. Yankin, O. M. Fedorova, I. A. Zvereva, S. G. Titova, and V. F. Balakirev. *Glass Phys. Chem.*, **2006**, *32*, 574.
10. A. B. Missyul, I. A. Zvereva, and T. T. M. Palstra. *Mater. Res. Bull.*, **2012**, *47*, 4156.
11. H. Nakano, N. Ishizawa, H. Sato, and N. Kamegashira. *Adv. Sci. Technol.*, **2010**, *67*, 113.
12. J. Meng, H. Satoh, M. Ishida, and N. Kamegashira. *J. Alloys Compd.*, **2006**, *408–412*, 1182.
13. S. A. Uporov, V. Ya. Mitrofanov, O. M. Fedorova, and A. M. Yankin. *Mater. Res. Bull.*, **2015**, *67*, 201.
14. D. Lee and H.N. Lee. *Materials*, **2017**, *10*, 368.
15. A. C. Larson and R. B. Von Dreele. General Structure Analysis System (GSAS). Los Alamos National Laboratory Report LAUR 86-748. Los Alamos, NM, **2004**.
16. G. Liu, T. T. Chen, J. Wang, X. Q. Liu, and X. M. Chen. *J. Alloys Compd.*, **2013**, *579*, 502.
17. I. S. Yakovleva, L. A. Isupova, and V. A. Rogov. *Kinet. Catal.*, **2009**, *50*, 275.
18. S. M. Pikalov, L. B. Vedmid', E. A. Filanova, E. Yu. Pikalova, J. G. Lyagaeva, N. A. Danilov, and A. A. Murashkina. *J. Alloys Compd.*, **2019**, *801*, 558.
19. S. V. Trukhanov, I. O. Troyanchuk, M. Hervieu, H. Szymczak, and K. Bärner. *Phys. Rev. B*, **2002**, *66*, 184424.
20. R. Seshadri, C. Martin, A. Maignan, M. Hervieu, B. Raveau, and C. N. Rao. *J. Mater. Chem.*, **1996**, *6*, 1585.